

THE EFFECT OF S-WAVE ARRIVAL TIMES ON THE ACCURACY OF HYPOCENTER ESTIMATION

BY JOAN S. GOMBERG, KAYE M. SHEDLOCK, AND STEVEN W. ROECKER

ABSTRACT

Well-constrained hypocenters (latitude, longitude, depth, and origin time) are required for nearly all studies that use earthquake data. We have examined the theoretical basis behind some of the widely accepted "rules of thumb" for obtaining accurate hypocenter estimates that pertain to the use of S phases and illustrate, in a variety of ways, why and when these "rules" are applicable. Results of experiments done for this study show that epicentral estimates (latitude and longitude) are typically far more robust with respect to data inadequacies; therefore, only examples illustrating the relationship between S phase arrival time data and focal depth and origin time estimates are presented. Most methods used to determine earthquake hypocenters are based on iterative, linearized, least-squares algorithms. Standard errors associated with hypocenter parameters are calculated assuming the data errors may be correctly described by a Gaussian distribution. We examine the influence of S-phase arrival time data on such algorithms by using the program HYPOINVERSE with synthetic datasets. Least-squares hypocenter determination algorithms have several shortcomings: solutions may be highly dependent on starting hypocenters, linearization and the assumption that data errors follow a Gaussian distribution may not be appropriate, and depth/origin time trade-offs are not readily apparent. These shortcomings can lead to biased hypocenter estimates and standard errors that do not always represent the true error. To illustrate the constraint provided by S-phase data on hypocenters determined without some of these potential problems, we also show examples of hypocenter estimates derived using a probabilistic approach that does not require linearization. We conclude that a correctly timed S phase recorded within about 1.4 focal depth's distance from the epicenter can be a powerful constraint on focal depth. Furthermore, we demonstrate that even a single incorrectly timed S phase can result in depth estimates and associated measures of uncertainty that are significantly incorrect.

INTRODUCTION

Well-constrained hypocenters (latitude, longitude, depth, and origin time) are required for studies of Earth structure, focal mechanisms, and the delineation of active tectonic features; indeed, the earthquake studies that do not require accurate hypocenters are few. The nonlinear nature of the problem of determination of an earthquake hypocenter makes it difficult to predict the response of the solutions to characteristics of the input data and parameters. However, the problem has been studied by many researchers and "rules of thumb" have been developed. These pertain to the number and configuration of recording stations, the starting hypocenter (Bolt, 1960; Nordquist, 1962; Cisternas, 1964; James *et al.*, 1969; Chatelain *et al.*, 1980), and the distribution and number of *P* and *S* phases (James *et al.*, 1969; Buland, 1976; Chatelain *et al.*, 1980; Ellsworth and Roecker, 1981). We present a summary of what these and other authors have learned about the sensitivity of hypocenter determination, particular focal depth, to the inclusion of *S* phases. These "rules of thumb" and the theoretical basis behind them are illustrated in a series of experiments using hypothetical data.

The approach that is most often taken to solve this nonlinear problem has been to linearize the relationship between travel time and location (Geiger, 1910). A truncated Taylor's series expansion of this relationship results in a problem in which travel-time residuals are linearly related to perturbations to some starting hypocenter. Mathematically, this is written as

$$\left(\frac{\partial T_k}{\partial \text{lon}}\right) \Delta \text{lon} + \left(\frac{\partial T_k}{\partial \text{lat}}\right) \Delta \text{lat} + \left(\frac{\partial T_k}{\partial z}\right) \Delta z + \Delta t_0 = \text{residual}_k \quad k = 1, 2, \dots, K \quad (1)$$

where the partial derivatives of travel time, T , with respect to longitude (lon), latitude (lat), depth (z), and origin time (t_0), respectively, are calculated for some starting hypocenter and the location of the station where the k th phase was recorded. K is the total number of phase arrival times used. The residual for the k th phase is the difference between the observed arrival time and the arrival time calculated for the starting hypocenter and station location where the phase was recorded.

All commonly used computer programs to perform earthquake hypocenter determination are based on this linearized approach [e.g., HYPO71 (Lee and Lahr, 1974), HYPOINVERSE (Klein, 1978), and HYPOELLIPSE (Lahr, 1979)]. The hypocenter solution or perturbations, Δlat , Δlon , Δz , Δt_0 , may be found using a variety of least-squares procedures (Flynn, 1960), such as step-wise multiple regression (Lee and Lahr, 1974), and singular value decomposition (Bolt, 1960; Buland, 1976; Klein, 1978). Regardless of which procedure is used, insight into the sensitivity of the hypocenter solution to the data (residuals) can be gained by forming the normal equations that correspond to equation (1) and examining the terms of the pseudo-inverse (Lawson and Hanson, 1974; see Appendix A). It then becomes apparent that a trade-off between depth and origin time can become significant when the depth partial derivatives are similar in magnitude and sign; in terms of data requirements this means that the phases used should have a variety of vertical slownesses or equivalently, take-off angles. When the constraints on depth and origin time are independent, the sensitivity of the origin time to all data is equal and constant, and for the depth, the sensitivity to each datum is proportional to the corresponding partial derivative (Ellsworth and Roecker, 1981). Thus, to obtain well-resolved depths and origin times, it is necessary to use a set of phase arrival times with a range of associated depth partial derivatives (Appendix A). When this is true, then those data with the largest associated depth partial derivatives will provide the strongest constraint on the focal depth.

Although the problem of hypocenter determination is usually solved using some form of linearized least-squares algorithm, the general characteristics of the relationship between P - and S -phase data and hypocenter estimates are not just a consequence of using linearized least-squares, but rather are controlled by the geometry and physics of the problem. Therefore, we will also examine this relationship without performing any linearization using the probabilistic formulation of Tarantola and Valette (1982; see also Tarantola, 1987). The basis of their approach is that the information about a model (the hypocenter contained in the vector \mathbf{m}) obtained from a set of data (arrival times contained in the vector \mathbf{t}), and an understanding of the underlying physics may be presented by the probability density function (p.d.f.), $P(\mathbf{m})$:

$$P(\mathbf{m}) = \Sigma(\mathbf{m}) \int_{-\infty}^{\infty} \frac{\Sigma(\mathbf{t})\Omega(\mathbf{t}|\mathbf{m})}{\mu(\mathbf{t})} d\mathbf{t}. \quad (2)$$

The vector notation is shorthand for

$$P(m_1, \dots, m_N) = \Sigma(m_1, \dots, m_N) \int_{-\infty}^{\infty} \int_{-\infty}^{\infty} \dots \int_{-\infty}^{\infty} \frac{\Sigma(t_1, \dots, t_K) \Omega(t_1, \dots, t_K | m_1, \dots, m_N)}{\mu(t_1, \dots, t_K)} dt_1 \dots dt_K. \quad (3)$$

In the problem of the hypocenter determination, the model vector \mathbf{m} has four elements, $N = 4$, and contains the hypocenter parameters

$$\mathbf{m} = [\text{lat}, \text{lon}, z, t_0]^T. \quad (4)$$

$\Sigma(\mathbf{m})$ represents any *a priori* information about the hypocenter (we only require that the focal depth be below the surface), $\Sigma(\mathbf{t})$ represents *a priori* information about the true (error-free) values of observables contained in vector \mathbf{t} (e.g., that the data are describable by a particular distribution function), $\Omega(\mathbf{t} | \mathbf{m})$ represents the conditional probability of predicting \mathbf{t} from an assumed model \mathbf{m} , and $\mu(\mathbf{t})$ describes the “state of ignorance” (we use $\mu(\mathbf{t}) = \text{constant}$, which means that all observations are equally possible).

It is also common knowledge that in the hypocenter determination problem there is a trade-off between changes in focal depth and origin time. Since this is not readily apparent from a least-squares solution, we examine the marginal p.d.f. that represents the probability of a particular spatial location given that all origin times are possible. The marginal p.d.f. is obtained by integrating equation (2) over all origin times, or

$$\tilde{P}(\text{lat}, \text{lon}, z) = \int_{-\infty}^{\infty} P(\text{lat}, \text{lon}, z, t_0) dt_0. \quad (5)$$

The use of $\tilde{P}(\text{lat}, \text{lon}, z)$ is sensible since we typically have no reason for favoring one origin time over another. It also allows us to explicitly include the effects of hypocenter/origin time trade-offs. The details of the calculation of $\tilde{P}(\text{lat}, \text{lon}, z)$ are presented in Appendix B.

RESULTS FROM THE LITERATURE

James *et al.* (1969) examined the instability resulting from using least-squares to solve for four-parameter hypocenter solutions when the recording networks are comprised of only a small number (<15) of stations. They put forth two key ideas about the accuracy of earthquake hypocenter determination:

1. locations determined for an earthquake whose true focal depth is less than half the average station separation will generally be inaccurate, and
2. since *S* phases are generally more difficult to accurately identify (particularly from vertical components), it is desirable to have several *S* readings.

Buland (1976) examined the precision and convergence properties of hypocenter determination algorithms by performing a series of numerical experiments. He noted that in all cases in which both *P* and *S* phases were used, convergence was superlinear (in linear convergence, the rms error decreases uniformly with each

iteration; in superlinear convergence, the rms error decrease accelerates with each iteration) and did not depend on the hypocenter chosen as the starting hypocenter. Buland's experiments also illustrated that the inclusion of *S*-phase arrivals yielded hypocenter estimates with smaller standard errors than those determined with only *P*-phase arrivals. However, as will be illustrated later, convergence to the correct solution cannot be guaranteed when there are systematic errors in the identification of *S* phases or introduced by use of an incorrect velocity model. In such cases, the standard errors do not necessarily reflect the true accuracy of the derived hypocenters.

Chatelain *et al.* (1980) performed a series of tests to determine the effects of the distance of recorded *P* and *S* phases on hypocenter accuracy. They used synthetic data and recordings of microearthquakes in a region of the Hindu Kush (area of approximately $4^\circ \times 4^\circ$) in a suite of experiments designed to examine the effects on hypocenter estimates of variations in Earth structure, random travel time errors, and variations in network geometry. They concluded that, in general, at least eight arrivals, of which at least one was an *S* phase, and at least one was reported from a station within a focal depth's distance from the earthquake, were minimal requirements for accurate hypocenter determination for their network.

Another demonstration of the strength of the *S* phase as a constraint on earthquake hypocenter determination can be made by examining its effect on the error ellipsoid. Urhammer (1982) demonstrated that, if the uncertainties in timing a *P* or *S* phase are approximately equal, then including one *S* phase in a dataset reduces the semi-major axis of the location error ellipsoid as much as including 1.7 *P* phases; the reason for this becomes clear in the next section of this paper. Uhrhammer (1982) made the same observation as James *et al.* (1969), that the uncertainties in timing *S* are generally greater than for *P*. Therefore, he concluded that they will have approximately equal effect in reducing the magnitude of the semi-major axis.

Ellsworth and Roecker (1981) discussed the importance of *S* phases in the linearized least-squares location problem by examining the partial derivatives (slowness vectors) of travel time with respect to focal depth and epicenter. The depth partial derivatives for *P* and *S* phases recorded at stations *k* and *j* are

$$\frac{\partial T_k^P}{\partial z} = \frac{\cos i_k^P}{v_p}, \quad \frac{\partial T_j^S}{\partial z} = \frac{\cos i_j^S}{v_s} \quad (6)$$

where *z* is the focal depth, v_p and v_s are the velocities, and T_k^P , i_k^P , and T_j^S , i_j^S are the travel times and take-off angles for *P* and *S* phases recorded at the *k*th and *j*th stations, respectively. To examine the relative contribution of an *S* phase in constraining the focal depth, we consider how a *P* phase can provide the same information. This is true when $\partial T_j^S/\partial z = \partial T_k^P/\partial z$ and the relation

$$\cos i_j^S = (v_s/v_p)\cos i_k^P \quad (7)$$

results. This equation shows that an up-going *S* phase with a take-off angle of $i_k^S = \cos^{-1}(v_s/v_p) \approx \pm 56^\circ$ (assuming a typical value of $v_p/v_s = 1.7$) will have a partial derivative that is equal to that of a vertically incident *P* phase. When $|i_j^S|$ is greater than about 56° and equation (7) is true, then an *S* phase is equivalent to a more vertically traveling *P* phase (in this case, $\cos i_k^S < v_s/v_p$, $\cos i_k^P$ must be less than $\cos i_j^S$, and $|i_k^P| > |i_j^S|$). Thus, an *S* phase can be thought of as a geometrically equivalent *P* phase that travels along a steeper ray path to a closer station.

Geometrically, phases recorded at closer stations improve depth control, so that we expect that inclusion of S will provide better depth constraints for a given geometry. Figure 1 schematically illustrates geometrically why recordings at stations close to the epicenter provide strong constraints.

Equation (7) also shows why an S can provide a unique constraint. When $|\cos i_j^s| > v_s/v_p$ ($|i_j^s| < 56^\circ$), then $(v_p/v_s)|\cos i_j^s| > 1$, which implies that $|\cos i_k^p| > 1$. Since the latter can never be true, there is no P phase with a take-off angle that results in as large a partial derivative as that for an S phase. In addition to providing a constraint on the hypocenter depth that is greater than any possible P phase, the uniqueness of the S partial derivative at these distances can significantly reduce the trade-off between depth and origin time (see Appendix A). The distances at which S is a unique constraint can be estimated by rewriting equation (6) in terms of source depth, z , and source-receiver distance, D (see

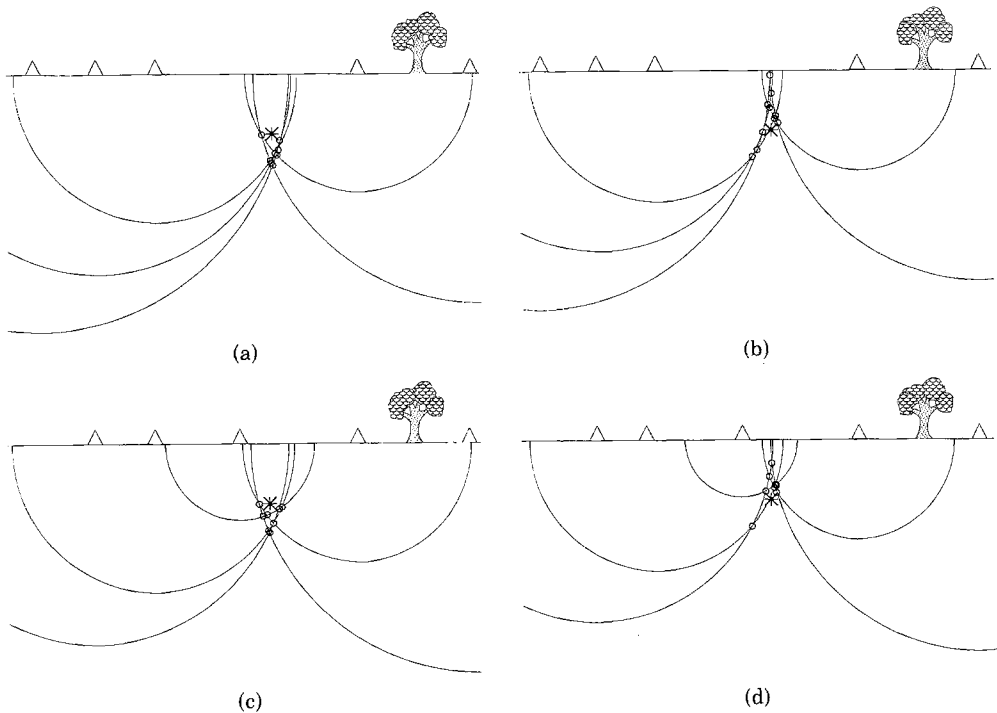


FIG. 1. (a) Locating an earthquake can be viewed as a triangulation problem. A measured travel time is converted to a distance using an assumed velocity model; for a homogeneous half-space, this distance defines a hemisphere of possible earthquake locations; the radius of the hemisphere is equal to the velocity multiplied by the travel time from source to receiver. For an exact velocity model, all such hemispheres drawn for travel times measured at a number of stations will intersect at a single point: the true hypocenter. Cross sections (semi-circles) of the hemispheres that result when the velocity is too fast, the origin time is too early, or the arrival times are all too late are shown in this figure. The true hypocenter is shown by the asterisk, the recording stations by the triangles, and the intersection points by the small circles. The location algorithm will determine a hypocenter that, in some sense, is an average of the intersection points; note that in this case the estimated depth will be deeper than the true depth. Also note that all the stations are located farther than 1.5 times the focal depth in distance. (b) The same as (a) except that the semi-circles are those that result if the velocity is too slow, the origin time is too late, or the arrival times are all too early. (c) The benefit of recording data within approximately a focal depth's distance from the true epicenter is illustrated here. One of the five stations shown in (a) has been moved and data are recorded within one focal depth's distance from the source. This results in a greater number of intersection points closer to the true hypocenter and thus, the estimated focal depth should lie closer to the true depth. The only way to double the number of these more accurate intersections is to use two (P and S) phase types (a single phase type recorded twice at closely spaced distances does not add independent information). (d) The same as (c) except that it corresponds to (b).

Fig. 2). For up-going rays, the cosine terms of the partial derivatives are

$$\cos i = z / \sqrt{z^2 + D^2} \quad (8)$$

and the equivalent criteria to $|\cos i_j^s| > v_s/v_p$ is that

$$D < z \sqrt{(v_p/v_s)^2 - 1} \quad (9)$$

or using a reasonable value of $(v_p/v_s)^2 = 3$,

$$D < 1.4z. \quad (10)$$

This is shown as the shaded region of Figure 2 and will be illustrated further in an example presented in the latter part of this paper.

For a P and an S phase recorded at the same station (equal take-off angles), the relation

$$\frac{\partial T_k^P}{\partial z} = \left(\frac{v_p}{v_s} \right) \frac{\partial T_j^S}{\partial z} \quad (11)$$

can be derived from equation (6). Thus, at a given station, the partial derivative for S is always larger than that for P by a factor of v_p/v_s , and the S phase is guaranteed

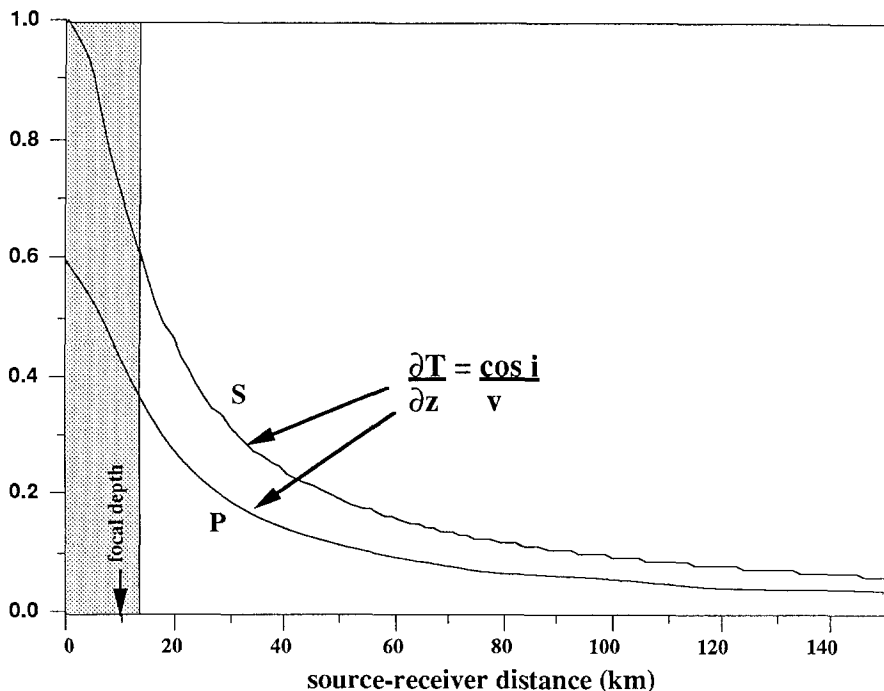


FIG. 2. Partial derivatives of travel time with respect to focal depth for P and S phases in a homogeneous half-space. A focal depth of 10 km is used. The derivatives are normalized so that the S derivative has a peak value of 1 (thus, the vertical axis is dimensionless). The shaded region indicates the distance range in which S provides a unique constraint. $\partial T/\partial z$ = partial derivative; T = time; z = depth; i = take-off angle (up-going ray with respect to vertical); v = P or S velocity.

to act as a unique constraint, thereby reducing the trade-off between depth and origin time (see Appendix A).

An S phase also can serve as a unique constraint and as a geometrically equivalent P phase for the determination of epicenters as well as focal depths (Ellsworth and Roecker, 1981). Following similar steps as previous paragraphs, examination of the partial derivatives of travel time with respect to latitude and longitude shows that the relationship between take-off angles for P and S phases is

$$\sin i_j^s = \frac{v_s}{v_p} \sin i_k^p. \quad (12)$$

When $|\sin i_j^s| \leq v_s/v_p$, an S phase acts geometrically as an equivalent P phase from a more distant station. As before, when recorded at the same distance an S phase is a stronger constraint since the S partial derivative is larger by a factor of v_p/v_s . When $|\sin i_j^s| > v_s/v_p$, the S phase serves as a unique constraint as there is no equivalent P phase. Thus, the recording of an S phase is potentially more valuable than recording a P phase, since S can provide unique information and is a stronger constraint on all three spatial parameters of a hypocenter.

It is also straightforward to show why in any approach that relies on satisfying arrival time data, the hypocenter that results in the best fit to data (using any sort of norm) will be the one that best satisfies the S rather than the P datum recorded at the same station. We examine density functions $P(\text{lat}, \text{lon}, z, t_0)$ that are proportional to

$$\exp - \left\{ \sum_{i=1}^N \frac{|g_i - t_i^{\text{obs}}|^q}{qS_i^q} \right\} \quad t_i^{\text{obs}} = t_i + e_i \quad (13)$$

where g_i is the i th theoretical arrival time, and the observed arrival time, t_i^{obs} , is the sum of the exact time, t_i , and the associated error, e_i . S_i is a measure of the spread corresponding to the i th datum (e.g., the variance in a Gaussian distribution), and $q = 2$ for Gaussian or $q = 1$ for exponential distributions. Linearized least-squares methods minimize the argument of the exponent of (13) assuming a Gaussian distribution (examples using both $q = 1$ or $q = 2$ are shown later); however, regardless of what q is, and if a P and S phase are recorded at the same station, it is easy to show that the minimum residual and hence, the highest probability, will be obtained by satisfying the S datum. If the hypocenter is determined such that the S datum is satisfied, the P residual will be

$$\frac{|(v_s/v_p)e_s - e_p|^q}{qS_p^q}. \quad (14)$$

(The suffixes p and s indicate the phase type.) Alternatively, if the P datum is satisfied, the S residual will be

$$\frac{|v_p/v_s((v_s/v_p)e_s - e_p)|^q}{qS_s^q}, \quad (15)$$

which is always larger than (14) by a factor of $|v_p/v_s|^q$ if the P and S spreads are equal.

EXAMPLES

Although the specific behavior of solutions to the earthquake location problem cannot be predicted, all of the conclusions just described share certain common features. These general features are illustrated in Figures 3 through 12, which show the results of several experiments performed with synthetic data. Synthetic arrival time data were generated for a simple, plane-layered structure for a suite of hypothetical earthquakes recorded by a hypothetical seismic network (Fig. 3). The hypothetical dataset consisted of 25 earthquakes (all with focal depths of 10 km) and 71 stations in an area of approximately $300 \times 350 \text{ km}^2$ (an average of 1 station per $38.5 \times 38.5 \text{ km}^2$). The number of *P* and *S* phase arrival times generated for each event is listed on the top of Figure 4; the station locations closest to each event were used in generating the corresponding synthetic dataset. Gaussian noise with a standard deviation of ± 0.02 sec was added to the arrival times to simulate any sort of random error (referred to as "noise" in the figures). These synthetic data were used as input to the program HYPOINVERSE (Klein, 1978). The initial epicenters were chosen to be the locations of the stations with the earliest arrivals, and the initial focal depths were all at 7 km. All phases were given the same weight initially and weights were calculated in HYPOINVERSE for each phase based on the derived source-receiver distances and travel-time residuals (arrivals at more distance stations and/or with large residuals are down-weighted). In order to illustrate that the

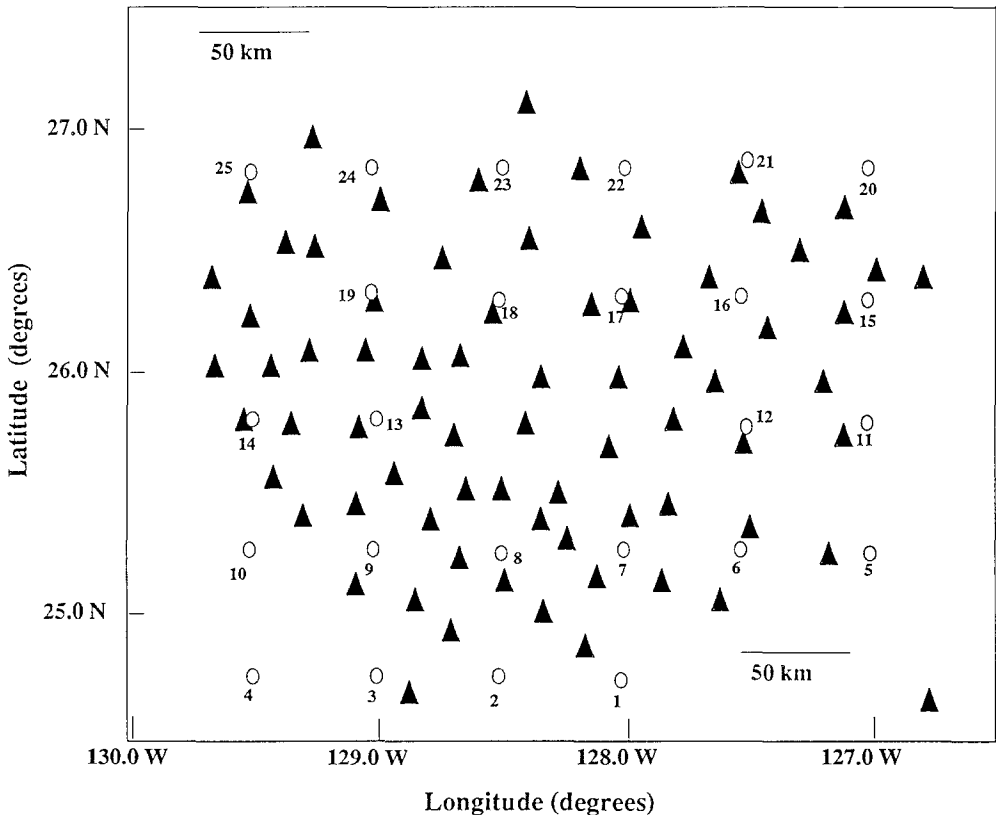


FIG. 3. Hypothetical seismic network and earthquake locations. All focal depths are at 10 km. Open circle = epicenter and event number (all focal depths are at 10 km); solid triangle = seismic station.

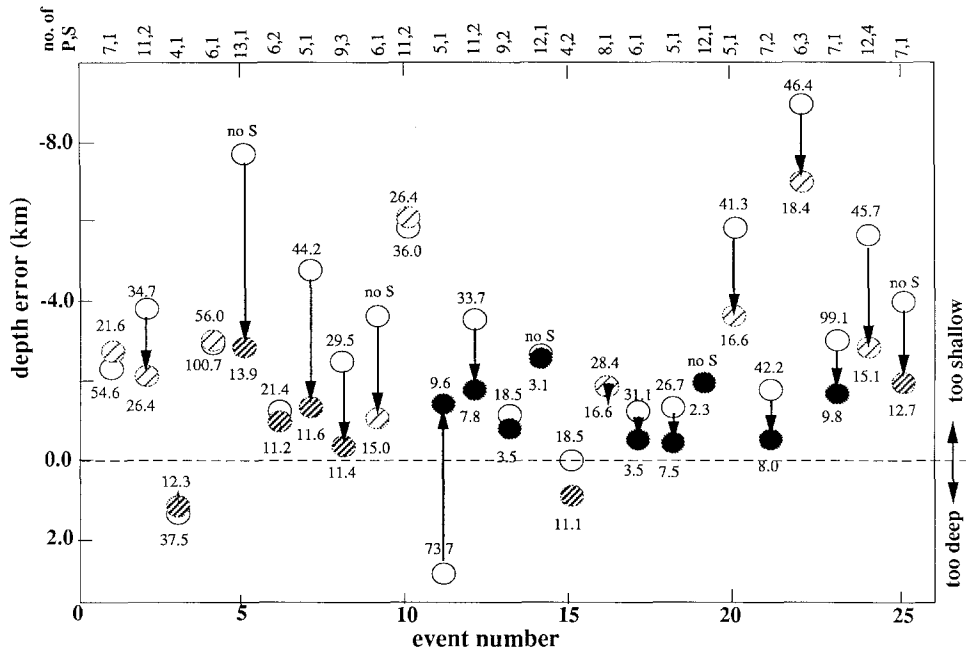


FIG. 4. Focal depth errors (calculated minus the true depth) for the 25 earthquakes in Figure 3. The velocity model used in HYPOINVERSE was 4 per cent faster than that used in the forward calculations. The number above or below each symbol is the distance (in kilometers) to the nearest station recording an *S* phase. Arrows are drawn in all cases in which a reduction in the error occurred as a consequence of recording an *S* closer to the event. Depth error when *S* is recorded at the closest station; symbols and distances to the closest station: solid circle = <1.0 focal depth; striped circle = between 1.0 and 1.4 focal depths; circle with clear band = >1.4 focal depths; open circle = depth error when there is no *S* recorded at the closest station.

benefit of recording an *S* phase close to the event is not just a consequence of solving the problem using a linearized least-squares algorithm, we also examine the marginal p.d.f., $\hat{P}(\text{lat}, \text{lon}, z)$, for several synthetic datasets.

The consequences of using a velocity model that has a systematic error are illustrated in Figures 4 through 8. A velocity model that was 4 per cent faster than that used to calculate the travel times was used to generate the results shown in Figures 4 through 8. While a 4 per cent error throughout may be larger than any overall systematic model error for most established networks (nonsystematic velocity model errors more appropriate to a well-studied region are discussed later), such error is certainly possible on a local scale, particularly since many seismically active regions are also regions with complex geology. Systematic model uncertainties of this magnitude are also quite possible in aftershock studies, as there may be little or no information about the true velocity structure in the region.

Figures 4 and 5 illustrate the importance of recording an *S* phase at a station located within approximately 1.4 focal depth's distance ("close"). Hypocenters were calculated initially using datasets that did not have an *S* phase at the closest station to the event. The open ovals are the focal depth errors that resulted for each event with the distance to the nearest station recording an *S* given directly above or below the oval. An *S* phase arrival at the closest station was then added to the dataset for each event and for those events that had at least one *S* previously, one *S* was removed. In most cases, the total number of *P* and *S* phases remained the same but one *S* phase was "moved" to the closest station to the event; in the remaining cases,

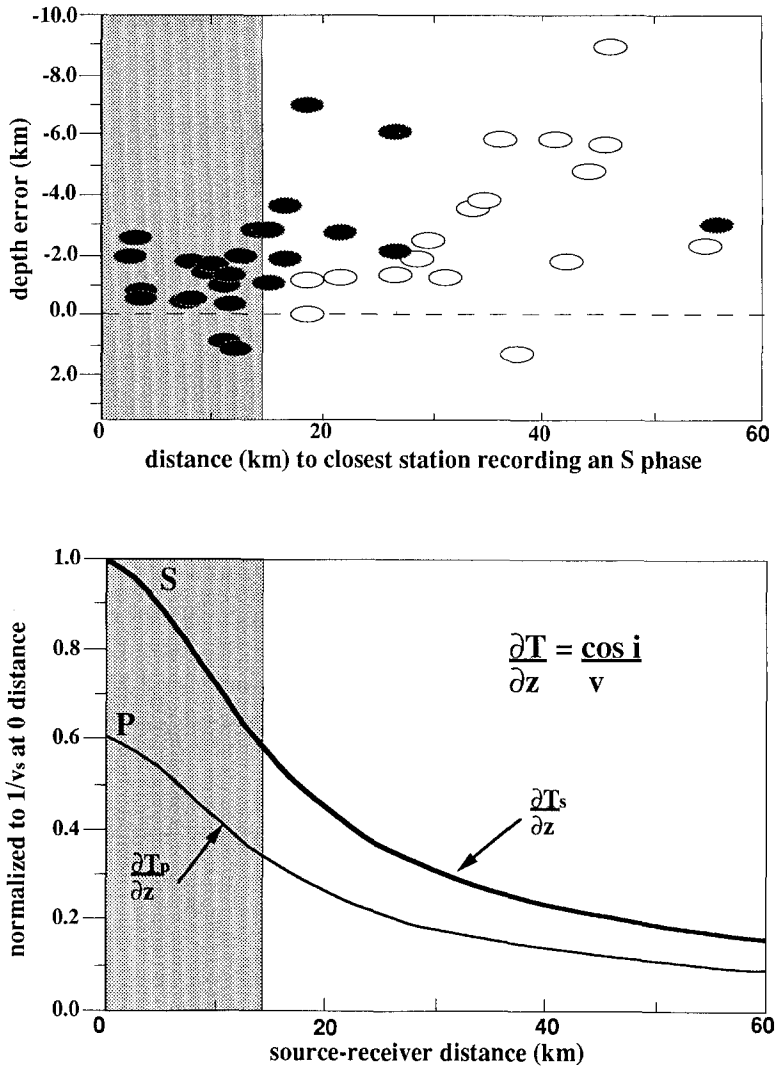


FIG. 5. The same focal depth errors shown in Figure 4 are compared with the depth partial derivatives (for a half-space) used in the least-squares algorithm (bottom). In the top figure, the open ovals are the same as those plotted in Figure 4 and indicate depth errors that result when an S phase arrival time from the closest station is not used to determine the hypocenter. The filled ovals are the same as the shaded ovals in Figure 4 and indicate the errors when an S datum at the closest station is used. The behavior of the partials with distance explains why the depths constrained by an S phase recorded within 1.4 focal depth's distance are consistently more accurate; at less than 1.4 focal depth's distance, the S constraint cannot be duplicated by any P phase. At the same distance an S phase provides 1.7 times the constraint provided by a P phase.

one S phase was added to the dataset. The filled ovals represent the focal depth errors that resulted using these new data; the distance to the nearest station (now recording an S phase) is given directly above or below the oval.

Nearly all events that are constrained by an S phase recorded close to the event showed improvement and have errors that are less than ± 2 km. Those events located on the perimeter of the network (Fig. 3) show the greatest percentage improvement since they were initially the most poorly constrained. When the distance to the nearest station recording S is greater than 1.4 focal depth's distance

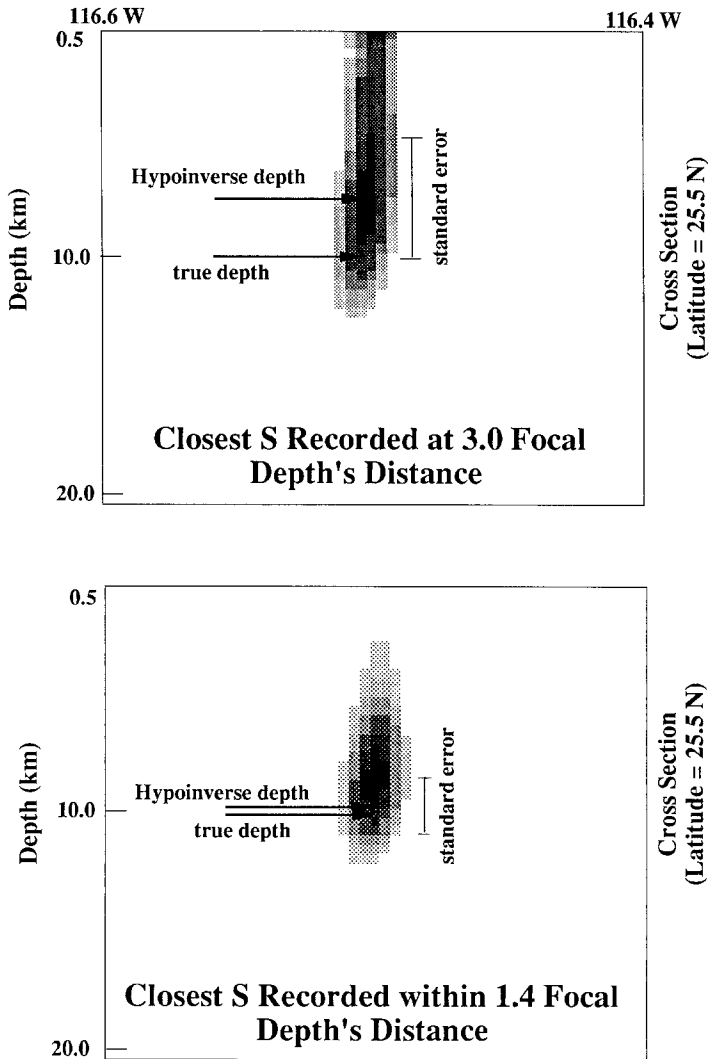


FIG. 6. A cross-section of the marginal p.d.f. $P(\text{lat}, \text{lon}, z)$ for event #8 (Figs. 3 and 4); the latitude is fixed at the latitude of the "true" epicenter. The shading is black when $P(\text{lat}, \text{lon}, z) > 90$ per cent of the peak value and changes every 10 per cent (becomes white at 40 per cent). A Gaussian density function is assumed in both cases (see Appendix B), and the velocity model is assumed is 4 per cent faster than that used to calculate the travel times. The station and phase distributions are the same for both cases except that the closest of the three S (nine P phases were also used) phases used was recorded at three focal depth's distance in the *top figure* and then "moved" to a station within 1.4 focal depth's distance for the *bottom figure*. Note that in the *top figure* both the least-square (HYPOINVERSE) solution with associated standard error and the marginal p.d.f. are badly biased. The latter also illustrates the trade-off between origin time and depth (indicated by the pencil-like shape of the p.d.f.). The *bottom figure* illustrates that recording S within a focal depth's distance reduces the sensitivity to the assumed velocity model and the trade-off between depth and origin time.

(events 1, 2, 4, 10, 16, 20, 22, and 24), there is little or no improvement. Events 14 and 19 have good azimuthal coverage, and no change is observed when an S phase is recorded at stations within 3.1 km of the events. However, note that there were 12 P phases for these two events (top of the figure) so that the constraint provided by the single S phase was simply "out-voted" by all the P data. This suggests that having lots of P phases is not necessarily an advantage, as it prevents the potentially

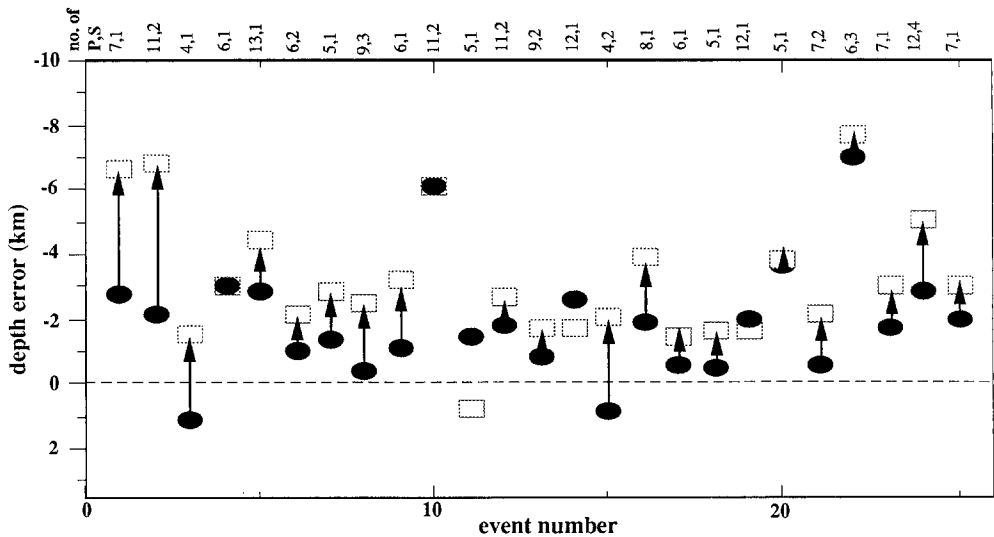


FIG. 7. Comparison of the focal depth errors that can occur when S is correctly identified and when a converted phase is mistaken for S . The filled ovals are the same as the shaded ovals of Figure 4, and the rectangles are the depth errors that result when a 0.2 sec (early) misidentification error is added to all the S phases. The arrows indicate less accurate focal depths that are a consequence of S phase misidentification.

more robust constraint provided by an S phase from having any effect on the derived focal depth.

Figure 5 shows the results of this experiment plotted such that the relationship between focal depth accuracy and distance to a station recording an S phase is clearer. It also corroborates the theoretical discussion presented earlier about the relative constraints provided by P and S phases as governed by the partial derivatives of travel time with respect to focal depth. The focal depth errors for each event are plotted as a function of the distance to the nearest station recording an S . The focal depth errors generally increase as the distance to the nearest station recording S increases. An increase in the magnitude of these depth errors occurs at approximately the same distance where S is no longer a unique constraint as indicated by the partial derivatives.

A cross-section of the marginal p.d.f., $\tilde{P}(\text{lat}, \text{lon}, z)$ for event 8 is shown in Figure 6, assuming that equation (5) is a Gaussian function [a model error of 0.38 sec was used, as it is the average difference in travel times calculated for the model used in the calculation of the data and for the faster model used to derive $\tilde{P}(\text{lat}, \text{lon}, z)$; see Appendix B for details]. The peak of $\tilde{P}(\text{lat}, \text{lon}, z)$ becomes much more localized around the true focal depth when S is recorded close to the event. This reduction in the bias is caused by the assumption of the wrong model and in the trade-off between focal depth and origin time. It illustrates the fundamental benefit of an S phase recorded within 1.4 focal depth's distance, which is independent of the method of hypocenter estimation.

In many networks an S phase must be measured from a vertical component as no horizontal components exist. Misidentification of a converted S -to- P phase as S will result in a systematic error such that the measured arrival time is earlier than the true arrival of the S phase. The consequences of this are demonstrated by using the same data as in Figures 4 and 5 (with an S phase at the closest station), but subtracting 0.2 sec from all S phases before deriving a location (Fig. 7). The accuracy

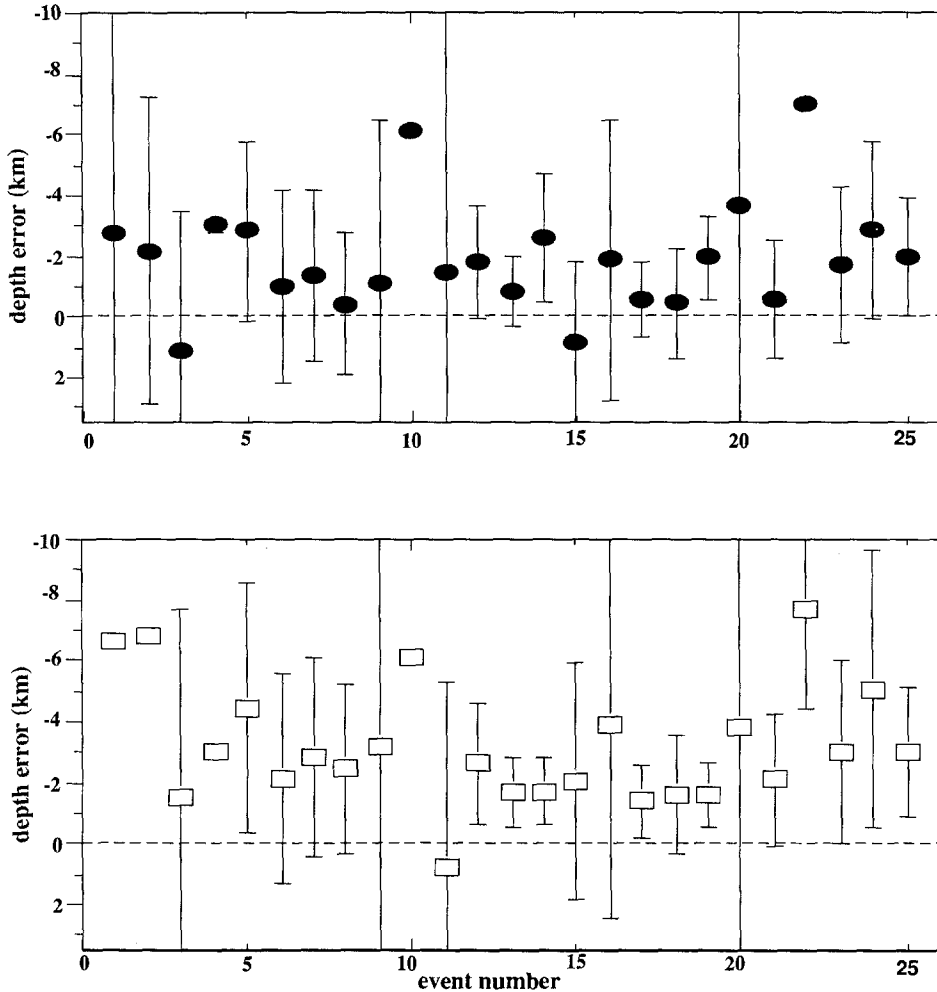


FIG. 8. The results plotted in Figure 4 are replotted in the *top graph*. The *bottom graph* shows the errors that result when *S* is systematically misidentified (e.g., if converted phases are large); the depth accuracy has decreased but one would judge them to be more accurate as the standard errors have decreased. This also leads to incorrect assessments about the validity of the assumed velocity model. Those points that have no error bars correspond to hypocenter solutions that became unstable such that the HYPOINVERSE algorithm fixed the depth during the iterative solution process.

of the focal depth estimates is degraded for all events with the exception of 11, 14, and 19. Unlike the previous case, the “out-voting” of the *S* phase by a large number of *P* phases for events 14 and 19 is advantageous, as it minimizes the effect of the erroneous *S*.

While misidentifying an *S* may cause a degradation in focal depth accuracy by a few kilometers, a more serious problem becomes apparent by examining the standard errors that are very often used to judge the quality of depth estimates. The standard errors produced in most location programs provide a measure of the solution precision, but as Figure 8 illustrates, the precision may have no bearing at all on the accuracy of the estimate. As Figure 7 illustrated, the inaccuracy of the estimates increased because of the erroneous *S* arrival times, but Figure 8 shows that, on average, the standard errors actually decreased. This is easy to understand by recalling that the velocity model used was too fast. The erroneous arrival times

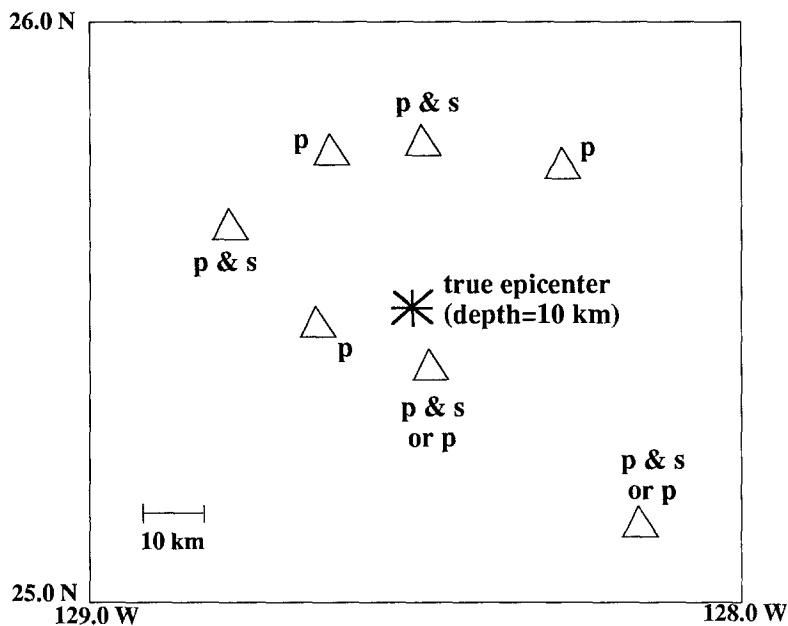


FIG. 9. The marginal probability distribution is examined for a typical situation in which there are fewer stations than for the example shown in Figure 6, the error in the velocity model is 1 per cent too fast, and the arrival times are not exact. The latter is simulated by adding Gaussian error (standard deviation of 0.1 sec, zero mean) to the calculated travel times.

were early, making them more like the times that would have been calculated if the correct model had been used. The travel-time residuals were reduced, a smaller rms error could be achieved, and smaller standard errors resulted. Thus, not only can phase misidentification cause greater inaccuracy in focal depth estimates, but it can also lead to development of erroneous velocity models. This example also provides an important lesson in the distinction between accuracy and precision; the latter is simply a measure of how closely measurements can be simulated regardless of the appropriateness of the closeness criteria or physical model invoked, and the former is a measure of the closeness of the estimate to the truth.

The necessity for correctly identifying and precisely measuring *S* phases is illustrated most clearly in Figures 9 to 11. Figure 9 shows the station/event configuration and phases used in the calculation of cross-sections of $\tilde{P}(\text{lat}, \text{lon}, z)$ shown in Figure 10; Gaussian "noise" (0.1 sec standard deviation) was added to exact travel times, and the model used was 1 per cent faster than that used in the calculation of the arrival times. This situation is similar to that of event 8 (example shown in Fig. 6), except that there are fewer stations and a smaller model error; this might be considered a more typical "real life" scenario. For purposes of illustration, an error of 0.4 sec was added to either the *P* or the *S* at the closest station, and we find that when the p.d.f. [equation (1)] is assumed to be a Gaussian, the marginal p.d.f. of equation (5) for either erroneous dataset is biased. The HYPOINVERSE estimates are also badly biased, and the least-squares estimation problem in the case with the *P* "outlier" becomes very nonlinear; the solution is dependent on the starting hypocenter and the standard errors do not represent the true error.

In Figure 11, we use all the same inputs as in Figure 10 but assume an exponential density function instead of a Gaussian since it has longer tails and thus, is more

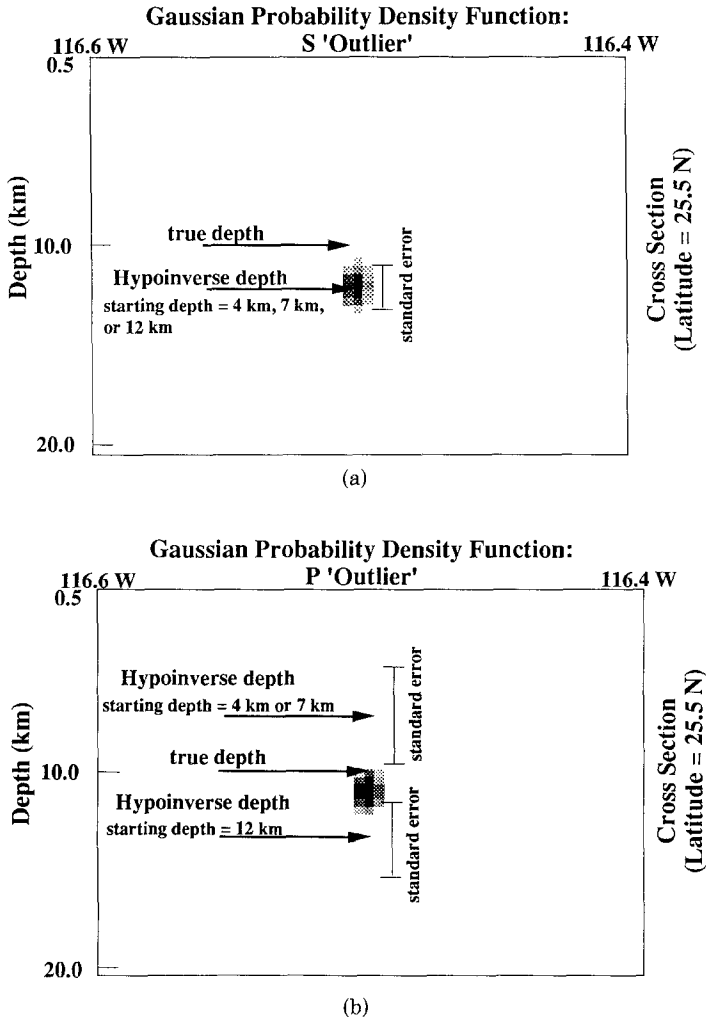


FIG. 10. (a) This example uses the data for the source/station distribution shown in Figure 9 with S recorded within 1.4 focal depth's distance (the closest station). Gaussian (0.1 sec standard deviation) "noise" has been added to the data, and the assumed model is 1 per cent too fast. At the closest station, an error of 0.4 sec has been added to the S travel time and the P time is exact. The S "outlier" seriously biases the p.d.f. and the HYPOINVERSE depth. This illustrates the nonrobust nature of a Gaussian distribution and a least-squares solution. (b) If the outlier corresponds to the P travel time rather than the S time, the bias in the p.d.f. is less severe; since S provides a greater constraint than P , hypocenter solutions are also more sensitive to errors in S . However, a P "outlier" causes the least-squares solution to become very nonlinear; it becomes very dependent on the choice of starting solution, and the standard errors do not represent the true error.

appropriate and robust in the presence of data outliers. The bias in $\tilde{P}(\text{lat}, \text{lon}, z)$ is eliminated for the dataset with the P outlier but changes insignificantly when there is an S outlier. This behavior is to be expected according to the discussion of equations (13) through (15), and illustrates that, even with a robust approach, the ill effects of erroneous S are extremely difficult to reduce. The spread of the S datum would have to be greater than that of the P by a factor of v_p/v_s (typically $\approx 1/\sqrt{3}$) or equivalently the S datum must be down-weighted by a factor of v_s/v_p to have an effect equal to that of P . In practice, S phase measurements cannot be made as accurately as those for P phases and will have larger spreads

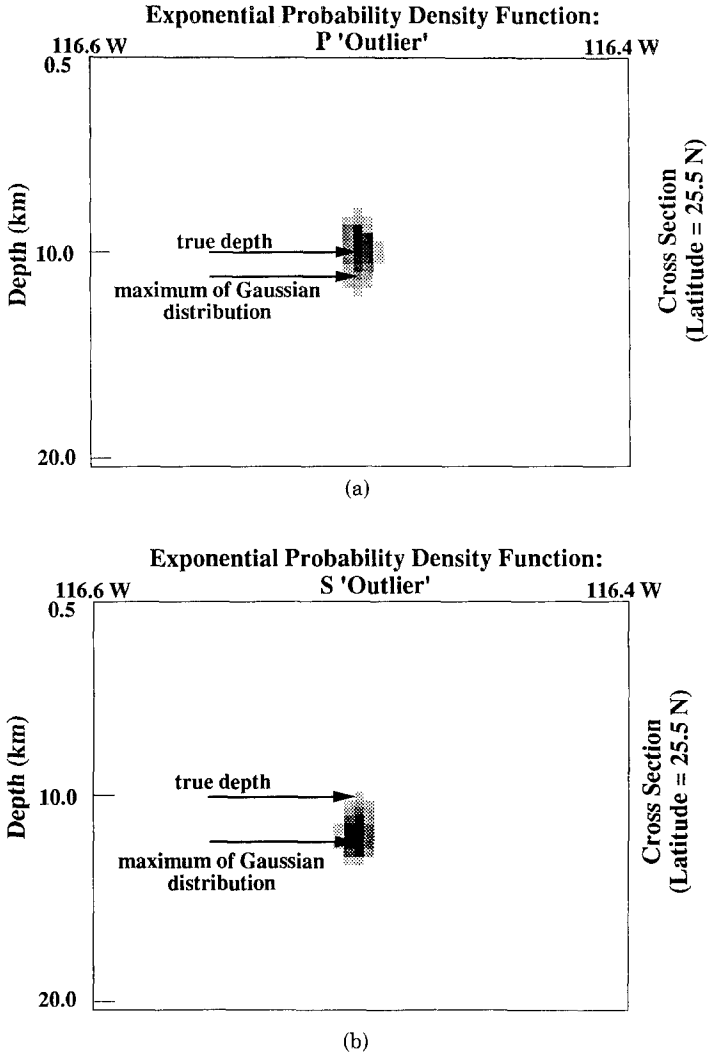


FIG. 11. The same data as in the previous examples are used here. However, an exponential marginal p.d.f. is used instead of a Gaussian; the exponential distribution is more robust with respect to data outliers. (A longer tailed distribution than a Gaussian is also probably more appropriate for real datasets; e.g., see Jeffreys, 1932; Buland, 1976). (b) The exponential distribution is more robust but only insignificantly so with respect to *S* outliers. The maxima of both the Gaussian and exponential distributions occur where the travel time residuals are minimized (in an L2 or L1 sense); when the *P* and *S* data are weighted identically (e.g., weights are equal to the variances for Gaussian distributions), the minimization is always optimized by satisfying the *S* travel time even if it is erroneous. This can lead to depth estimates that are very stable and very inaccurate!

assigned to them. While this does reduce the sensitivity to erroneous *S*, it also reduces the magnitude of the constraint that correct *S* readings can provide.

Figure 12 illustrates the importance of recording *S* phases when the vertically averaged velocity model is correct. The velocity model used in HYPOINVERSE was too fast by 2.9 per cent in the upper 3 km and too slow by 1.3 per cent below this so that the vertical travel time from a 10 km focus was the same as for the correct model. The plots at the top and bottom of Figure 12 follow the same format as Figures 4 and 5, respectively. The magnitude of the depth errors is reduced with respect to those resulting when there is a systematic velocity model error but the

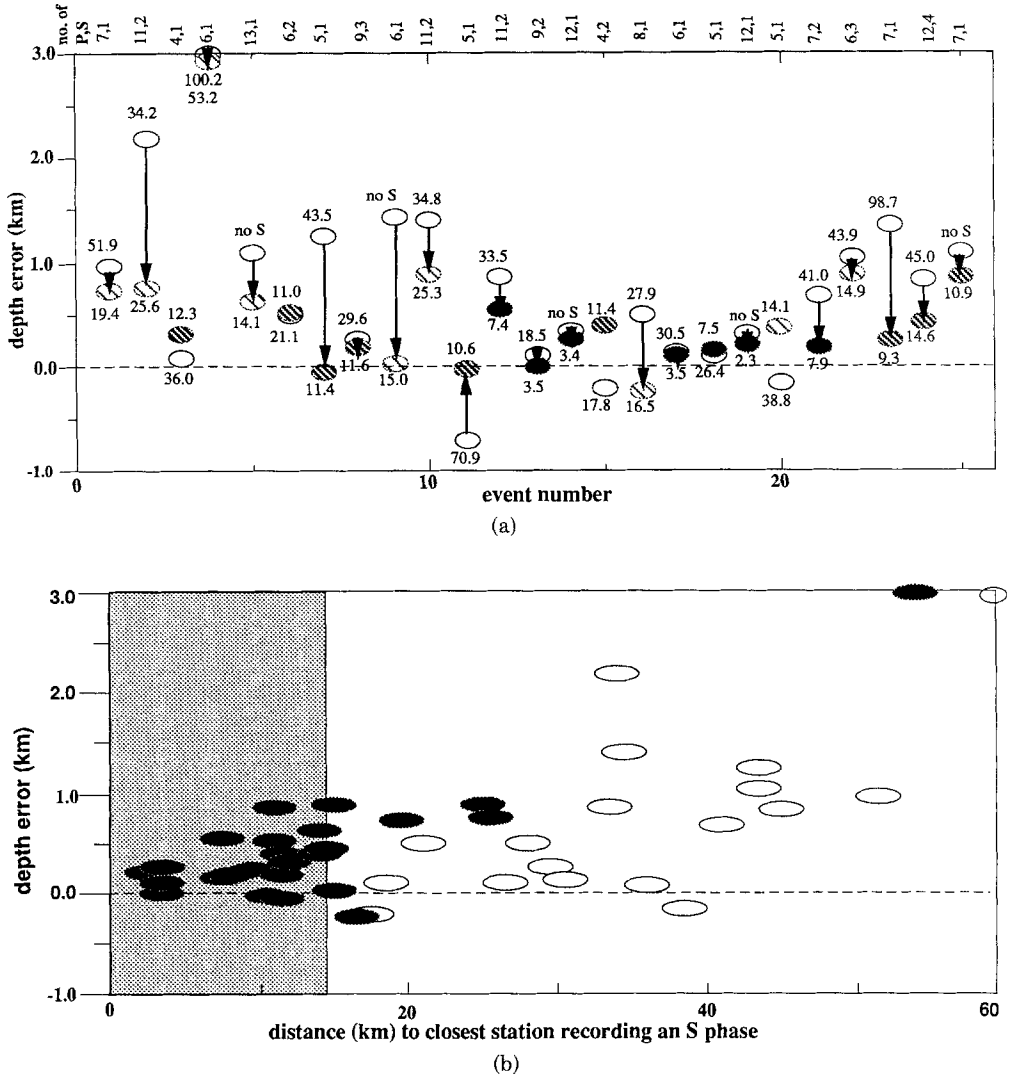


FIG. 12. (a) Focal depth errors (calculated depth minus true depth) for the 25 hypothetical earthquakes recorded at the hypothetical network shown in Figure 3. The velocity model used in HYOINVERSE was 2.9 per cent faster in the upper 3 km and 1.3 per cent slower below this than the model used to calculate the travel times. The vertical travel time for both models was the same. The open ovals are the errors that result when no *S* phase is recorded at the closest station. The format and labeling are the same as for Figure 4. The open and filled ovals corresponding to event 4 actually have depth errors of 6.2 and 5.9 km, respectively. (b) The same depth errors plotted as a function of the distance to the nearest station recording an *S* phase. The shaded area is the distance range in which *S* phases are unique constraints (see Fig. 2). Depth error when *S* is recorded at the closest station; symbols and distances to the closest station: solid circle = <1.0 focal depth; striped circle = between 1.0 and 1.4 focal depths; circle with clear band = >1.4 focal depths; open circle = depth error when there is no *S* recorded at the closest station.

inclusion of *S* phases has the same effect as in the previous examples. It improves the focal depth accuracy in nearly all cases, particularly at the perimeters of the network where the constraints provided by the other data are poor.

One property of nonlinear problems such as hypocenter determination is the unpredictability of the response of solutions to small changes in input parameters (e.g., small, localized deviations in model parameters from the real structure). Even

when the problem of hypocenter estimation is posed in such a way that linearization is not required, the influence of incorrect Earth structure and data errors can dominate the behavior of hypocenter solutions. Thus, for seismic networks meant to monitor seismicity confined to the upper crust, if the regional Earth structure is not known everywhere to within an uncertainty of less than a few per cent, then the only way to ensure that depth estimates will have uncertainties of no more than approximately 1.5 km is to record *S* phases within approximately 1.4 focal depth's distance. However, the *S* data must be correctly identified and timed with uncertainties of no more than approximately one tenth of a second.

CONCLUSIONS

The "rules of thumb" that we have illustrated may be summarized as follows.

- At least one *S* phase recording is required at a station within approximately 1.4 focal depth's distance from the source (hereafter, a phase recorded within this distance range will be called "close") to derive a focal depth that is accurate to within approximately ± 1.5 km. This criterion can be relaxed slightly when the vertically averaged velocity model assumed in the location procedure differs from the true velocity structure by less than a few percent.
- When systematic model errors are of the order of 4 per cent and there are no *S* phases recorded close to the source, then depth errors can be greater than approximately ± 3 km even when there is good azimuthal coverage and several *P* phases are recorded at less than a focal depth's distance. As the model error becomes less systematic and/or smaller in magnitude, the size of the depth errors also decreases. However, recording an *S* phase close to the event almost always improves the accuracy of depth determinations; in the absence of detailed knowledge of the regional velocity structure, the most certain way to minimize the solution's sensitivity to model parameters and theoretical simplifications is to record *S* phases within the aforementioned distance range.
- Recording an *S* phase close to an event is especially important when there is poor azimuthal coverage; the greatest relative improvement in focal depth accuracy is achieved in such cases.
- Recording *S* and *P* phases at a close station significantly reduces the trade-off between focal depth and origin time.
- Systematic *S* phase timing errors of 0.2 sec in magnitude (due to mistaken identification of a converted phase as *S*) can degrade focal depth estimation accuracy by several kilometers even when azimuthal coverage is good. Such errors can also result in a *reduction* in the standard errors; an apparent increase in *precision* can actually be associated with a decrease in *accuracy*! Furthermore, such systematic errors could lead to construction of incorrect velocity models.
- Because *S* is such a potentially powerful constraint, a single "bad" *S* at a close station can result in a very stable, yet very wrong solution even when robust methods of hypocenter determination are used.

This study, and the earlier studies cited in this paper, all provide strong evidence for the need to correctly identify and time *S* phases to ensure accurate hypocenter determination. The "rules of thumb" outlined here have serious implications for seismic network design. The first implication is that the optimal station spacing is such that seismographs be separated by no more than three times the depth of the most shallow earthquakes for which accurate depth estimates are required. Accurate identification and timing of an *S*-phase arrival can be accomplished with greatest

confidence if it is on a transverse component and from a seismogram that remains on scale. Therefore, the second and third implications are that network instrumentation should include two orthogonal horizontal components and should have sufficient dynamic range to not saturate in the relevant magnitude range. If all these criteria are satisfied, then nearly all hypocenters could be determined with sufficient accuracy for any study. In this way, the potential information that can be obtained from the data will be maximized.

ACKNOWLEDGMENTS

The authors would like to acknowledge Gil Bollinger, Geof King, and John Lahr for their thorough and constructive reviews. We also want to thank Bill Ellsworth for his early contributions. Finally, Dave Perkins deserves a thanks for participating in many helpful discussions.

REFERENCES

- Bolt, B. A. (1960). The revision of earthquake epicenters, focal depths, and origin times using a high-speed computer, *Geophys. J. Royal Ast. Soc.* **3**, 433-440.
- Buland, R. (1976). The mechanics of locating earthquakes, *Bull. Seism. Soc. Am.* **66**, 173-187.
- Chatelain, J. L., S. W. Roecker, D. Hatzfeld, and P. Molnar (1980). Microearthquake seismicity and fault plane solutions in the Hindu Kush region and their tectonic implications, *J. Geophys. Res.* **85**, 1365-1387.
- Cisternas, A. (1964). Precision determination of focal depths and epicenters of earthquakes, *CIT Publication*, AFOSR Contract No. AF-49(638) 1337.
- Ellsworth, W. L. and S. W. Roecker (1981). Sensitivity of the earthquake location problem to network geometry, in *Seismicity and Tectonics of the Pamir-Hindu Kush Region of Central Asia*, Ph.D. Thesis, MIT, Boston, Massachusetts, 296 pp.
- Flynn, E. A. (1960). Local earthquake location with an electronic computer, *Bull. Seism. Soc. Am.* **50**, 467-470.
- Gieger, L. (1910). Hedbestimmung bie erdbeben aus den ankunftszeiten, *K. Gessel. Wiss. Goett* **4**, 331-349.
- James, D. E., I. S. Sacks, E. Lazo, and G. Araracio (1969). On locating local earthquakes using small networks, *Bull. Seism. Soc. Am.* **59**, 1201-1212.
- Klein, F. (1978). Hypocenter location program Hypoinverse, *U.S. Geol. Surv., Open-File Rept.* 78-694, 113 pp.
- Lahr, J. C. (1979). A computer program for determining earthquake hypocentral parameters, magnitudes, and first motion patterns, *U.S. Geol. Surv., Open-File Rept.* 79-0431, 313 pp.
- Lawson, C. L. and R. J. Hanson (1974). *Solving Least Squares Problems*, Prentice-Hall, Englewood Cliffs, New Jersey, 340 pp.
- Lee, W. H. K. and J. C. Lahr (1974). HYPO71 (revised): a computer program for determining hypocenter, magnitude and first motion patterns of local earthquakes, *U.S. Geol. Surv., Open-File Rept.* 75-311, 114 pp.
- Nordquist, J. M. (1962). A special-purpose program for earthquake location with an electronic computer, *Bull. Seism. Soc. Am.* **52**, 431-437.
- Roecker, S. W., J. L. Chatelain, B. L. Isacks, and R. Prevot (1988). Anomalous deep earthquakes beneath the New Hebrides Trench, *Bull. Seism. Soc. Am.* **78**, 1984-2007.
- Tarantola, A. (1987). *Inverse Problem Theory; Methods for Data Fitting and Model Parameter Estimation*, Elsevier Science Publishing Co., Inc., New York, 613 pp.
- Tarantola, A. and B. Valette (1982). Inverse problems = quest for information, *J. Geophys.* **50**, 159-170.
- Urhammer, R. A. (1982). The optimal estimation of earthquake parameters, *Phys. Earth Plan. Interiors* **4**, 1369-1379.

U.S. GEOLOGICAL SURVEY
MS 966, BOX 25046
DENVER FEDERAL CENTER
DENVER, COLORADO 80225
(J.S.G., K.M.S.)

RENSELAER POLYTECHNIC INSTITUTE
DEPARTMENT OF GEOLOGY
TROY, NEW YORK 12180-3590
(S.W.R.)

APPENDIX A

The mathematical basis of the least-squares hypocenter estimation problem is summarized in this Appendix. The emphasis of the summary is on the influence of the partial derivatives as they pertain to trade-offs between depth and origin time, and how well they constrain either of these parameters. The formulations presented may be found in greater detail in Ellsworth and Roecker (1981). In situations where there is a significant trade-off between origin time and depth, the constraint on either parameter provided by a single datum is not proportional to the corresponding partial derivatives but, instead, to the sum of the partial derivatives or their squares, corresponding to all the data. The trade-off is minimized when there is a range in the magnitude and sign of depth partial derivatives which, in terms of data requirements, means that the phases used should have a variety of vertical slownesses or take-off angles. When the constraints on depth and origin time are independent, the sensitivity of the origin time to all data is equal and constant, and for the depth the sensitivity to each datum is proportional to the corresponding partial derivative. Thus, in this case, phase arrival times with larger associated depth partial derivatives, or equivalently having greater vertical slownesses or more vertical take-off angles, will provide greater constraint on the depth.

Mathematically, the linearized least-squares hypocenter estimation problem to solve can be written as

$$\left(\frac{\partial T_k}{\partial \text{lon}}\right) \Delta \text{lon} + \left(\frac{\partial T_k}{\partial \text{lat}}\right) \Delta \text{lat} + \left(\frac{\partial T_k}{\partial z}\right) \Delta z + \Delta t_0 = \text{residual}_k \quad k = 1, 2, \dots, K \quad (\text{A1})$$

where the partial derivatives of travel time with respect to longitude (lon), latitude (lat), depth (z), and origin time (t_0), respectively, are calculated for some starting hypocenter and the location of the station where the k th phase was recorded. K is the total number of phase arrival times used. The residual for the k th phase is the difference between the observed arrival time and the arrival time calculated for the starting hypocenter and station location where the phase was recorded.

In matrix form, equation (A1) can be written as

$$A\mathbf{m} = \mathbf{r} \quad (\text{A2})$$

where the vector $\mathbf{m} = [\Delta \text{lat}, \Delta \text{lon}, \Delta z, \Delta t_0]^T$, \mathbf{r} contains the residuals and A contains the partial derivatives. The normal equations that correspond to equation (A2) are written in matrix form as

$$A^T A \mathbf{m} = A^T \mathbf{r}. \quad (\text{A3})$$

If the following terms of $A^T A$ are zero,

$$\sum_{k=1}^K \frac{\partial T_k}{\partial \text{lon}} = 0, \quad \sum_{k=1}^K \frac{\partial T_k}{\partial \text{lat}} = 0, \quad \sum_{k=1}^K \frac{\partial T_k}{\partial \text{lon}} \frac{\partial T_k}{\partial z} = 0, \quad \sum_{k=1}^K \frac{\partial T_k}{\partial \text{lat}} \frac{\partial T_k}{\partial z} = 0, \quad (\text{A4})$$

then the problems of estimating the epicenter and origin time/depth decouple. The partial derivatives have the form

$$\frac{\partial T_k}{\partial z} = \frac{\cos i_k}{v}, \quad \frac{\partial T_k}{\partial t_0} = 1, \quad \frac{\partial T_k}{\partial \text{lat}} = \frac{\cos \phi_k \sin i_k}{v}, \quad \frac{\partial T_k}{\partial \text{lon}} = \frac{\sin \phi_k \sin i_k}{v} \quad (\text{A5})$$

where i_k and ϕ_k are the take-off angle and azimuth from the source to the k th station, respectively, and v is the material velocity. The conditions represented by equation (A4) will be approximately satisfied if the stations are nearly evenly distributed azimuthally around the epicenter, and the depth/origin time estimation problem can then be treated separately. Note that the depth, latitudinal, and longitudinal partial derivatives also represent the vertical and horizontal components of slowness, $1/v$.

In order to understand how the data (residuals) constrain the depth and origin time, the pseudo-inverse, $A^\dagger = (A^T A)^{-1} A^T$, must be formed (Lawson and Hanson, 1974). Since the requirements for decoupling of the epicenter and the depth/origin time estimation problem are often nearly satisfied, only the decoupled normal equations for the latter are considered. The relationship between the data and depth and origin time becomes

$$\mathbf{m}' = A^\dagger \mathbf{r} \tag{A6}$$

where $\mathbf{m}' = [t_0, z]^T$. The k th column of A^\dagger is

$$\frac{1}{\det(A^T A)} \begin{vmatrix} \sum_{i=1}^K \left(\frac{\partial T_i}{\partial z} \right)^2 - \frac{\partial T_k}{\partial z} \sum_{i=1}^K \left(\frac{\partial T_i}{\partial z} \right) \\ K \left(\frac{\partial T_k}{\partial z} \right) - \sum_{i=1}^K \left(\frac{\partial T_i}{\partial z} \right) \end{vmatrix} \tag{A7}$$

where K is the number of residuals. The top and bottom terms describe the sensitivity to origin time and depth, respectively. When these two terms are similar, there will be a trade-off between depth and origin time; the trade-off will be complete when

$$\left[\sum_{i=1}^K \left(\frac{\partial T_i}{\partial z} \right) \right]^2 = K \sum_{i=1}^K \left(\frac{\partial T_i}{\partial z} \right)^2. \tag{A8}$$

This condition becomes more nearly true as the partial derivatives become more similar to one another; geometrically, this corresponds to the situation where all the rays have similar vertical component slownesses. The trade-off will be minimized when the residuals correspond to up- and down-going rays so that the partials are of opposite sign and thus, cancel in the left-hand term of equation (A8).

When there is no trade-off between depth and origin time, the k th column of A^\dagger becomes

$$\begin{vmatrix} 1/K \\ \frac{\partial T_k / \partial z}{\sum_{i=1}^K (\partial T_i / \partial z)^2} \end{vmatrix}. \tag{A9}$$

This implies that the sensitivity of the origin time to all data is a constant and the sensitivity of the depth to each datum is proportional to the corresponding depth partial derivative. Thus, in this case, data having larger partial derivatives will provide greater constraint on the depth estimate.

APPENDIX B

The basis of the probabilistic approach of Tarantola and Valette (1982) (see also Tarantola, 1987) is that the information about a model that can be obtained from a set of data and an understanding of the underlying physics may be represented by the probability density function $P(\mathbf{m})$:

$$P(\mathbf{m}) = \Sigma(\mathbf{m}) \int_{-\infty}^{\infty} \frac{\Sigma(\mathbf{t})\Omega(\mathbf{t}|\mathbf{m})}{\mu(\mathbf{t})} d\mathbf{t}. \quad (\text{B1})$$

In the problem of hypocenter determination, the vector \mathbf{m} contains the hypocenter parameters

$$\mathbf{m} = [\text{lat}, \text{lon}, z, t_0]^T \quad (\text{B2})$$

where lat, lon represent the epicenter, z is the focal depth, and t_0 is the origin time. $\Sigma(\mathbf{m})$ represents any *a priori* information about the model; the only *a priori* information we use is that for all values of lat, lon, and t_0

$$\Sigma(\mathbf{m}) = \begin{cases} 1 & \text{for } z > 0, \\ 0 & \text{for } z \leq 0 \end{cases} \quad (\text{B3})$$

(focal depths must be below the surface). $\mu(\mathbf{t})$ describes the “state of ignorance;” the most noninformative probability ascribes the same likelihood to observing any datum or

$$\mu(\mathbf{t}) = Q \quad (\text{B4})$$

where Q is a constant. $\Sigma(\mathbf{t})$ represents *a priori* information about the true (error-free) values of observables contained in vector \mathbf{t} (that the observed data are describable by a particular distribution function), and $\Omega(\mathbf{t}|\mathbf{m})$ represents the conditional probability of predicting \mathbf{t} from an assumed model \mathbf{m} (the assumed physics and a description of the accuracy to which it represents the true process). Combining equations (B1) through (B4), equation (B1) becomes

$$P(\mathbf{m}) = Q \int_{-\infty}^{\infty} \Sigma(\mathbf{t})\Omega(\mathbf{t}|\mathbf{m}) d\mathbf{t}. \quad (\text{B5})$$

In order to explicitly include effects of trade-offs between origin time and focal depth, we examine the marginal probability, $\tilde{P}(\mathbf{m})$, which can be written

$$\tilde{P}(\mathbf{m}) = \int_{-\infty}^{\infty} P(\text{lat}, \text{lon}, z, t_0) dt_0. \quad (\text{B6})$$

When the *a priori* data and conditional probabilities, $\Sigma(\mathbf{t})$ and $\Omega(\mathbf{t}|\mathbf{m})$ respectively, are both Gaussian, equation (B5) can be integrated analytically (see Tarantola and Valette, 1982; Roecker *et al.*, 1988 for details). More explicitly, it

becomes

$$P(\text{lat}, \text{lon}, z, t_0) = Q \exp \left\{ - \left[\frac{(\mathbf{t}^{\text{obs}} - \mathbf{g})^T (C^t + C^m)^{-1} (\mathbf{t}^{\text{obs}} - \mathbf{g})}{2} \right] \right\} \quad (\text{B7})$$

where \mathbf{t}^{obs} contains the observed arrival times, the theoretical arrival times are contained in the vector \mathbf{g} , and C^t and C^d are the data and model covariance matrices, respectively. The marginal probability of equation (B6) becomes

$$\tilde{P}(\text{lat}, \text{lon}, z) = \tilde{Q} e \left(- \frac{\beta^2}{2} \right) \quad (\text{B8})$$

where

$$\beta^2 = (\tilde{\mathbf{t}}^{\text{obs}} - \tilde{\mathbf{h}})^T (C^t + C^m)^{-1} (\tilde{\mathbf{t}}^{\text{obs}} - \tilde{\mathbf{h}}) \quad (\text{B9})$$

\tilde{t}_i^{obs} is the i th demeaned arrival time, and \tilde{h}_i is the i th demeaned theoretical travel time,

$$\tilde{t}_i^{\text{obs}} = t_i^{\text{obs}} - \frac{\sum_{j=1}^K (C_{ij}^t + C_{ij}^m)^{-1} t_j^{\text{obs}}}{\sum_{j=1}^K (C_{ij}^t + C_{ij}^m)^{-1}}$$

and

(B10)

$$\tilde{h}_i = h_i - \frac{\sum_{j=1}^K (C_{ij}^t + C_{ij}^m)^{-1} h_j}{\sum_{j=1}^K (C_{ij}^t + C_{ij}^m)^{-1}}$$

and

$$\tilde{Q} = \sum_{i=1}^K \sum_{j=1}^K (C_{ij}^t + C_{ij}^m)^{-1}. \quad (\text{B11})$$

K is the total number of data. In all cases, we assume that errors in the data and, due to inadequate theoretical assumptions, are all uncorrelated. It is also assumed that the latter are equal for all theoretical calculations. When this is true, C^t becomes diagonal such that each diagonal term represents the variance of an individual phase arrival time measurement, and C^m is equal to the identity matrix multiplied by a constant variance attributed to forward modeling errors.

Use of an exponential density function is more robust with respect to data outliers; in this case, we assume that equation (B5) is appropriately represented by

$$P(\text{lat}, \text{lon}, z, t_0) = \exp - \left[\sum_{i=1}^K \frac{|g_i - t_i^{\text{obs}}|}{S_i} \right] \quad (\text{B12})$$

where t_i^{obs} , g_i , and K are the same as in the Gaussian case above, and S_i is a measure of the uncertainty of the i th datum. Although we have not explicitly defined the individual terms of the integrand of equation (B5) and integrated, the assumption

of (B12) is no less valid than assuming Gaussian functions. The latter as is usually done because it is mathematically convenient but is usually not verified observationally. Use of a longer-tailed distribution such as an exponential is probably more appropriate as suggested in several studies that actually examined the distribution of travel-time residuals [Jeffreys, 1932; Buland, 1976]. The exponential marginal p.d.f. of equation (B6) can be derived analytically and written as

$$\tilde{P}(\text{lat}, \text{lon}, z) = b^{-1} [e^{(-a+br_1)} + e^{(a-br_K)}] + e^a \sum_{i=1}^{K-1} \{c_i^{-1} e^{-d_i} [e^{-c_i r_i} - e^{-c_i r_{i+1}}]\} \quad (\text{B13})$$

where

$$r_i = t_i^{\text{obs}} - h_i, \quad r_1 < r_2 < \dots < r_K$$

$$a = \sum_{i=1}^K \frac{r_i}{S_i}, \quad b = \sum_{i=1}^K \frac{1}{S_i}, \quad c_i = b - 2 \sum_{n=i+1}^K \frac{1}{S_n}, \quad d_i = 2 \sum_{n=i+1}^K \frac{r_n}{S_n} \quad (\text{B14})$$

and h_i is the theoretical travel time ($g_i = h_i + t_0$).